LETTERS

Observation of the two-channel Kondo effect

R. M. Potok[1,3]†, I. G. Rau[2], Hadas Shtrikman[4], Yuval Oreg[4] & D. Goldhaber-Gordon[1]

Some of the most intriguing problems in solid-state physics arise when the motion of one electron dramatically affects the motion of surrounding electrons. Traditionally, such highly correlated electron systems have been studied mainly in materials with complex transition metal chemistry[1,2]. Over the past decade, researchers have learned to confine one or a few electrons within a nanometre-scale semiconductor 'artificial atom', and to understand and control this simple system in detail[3]. Here we combine artificial atoms to create a highly correlated electron system within a nano-engineered semiconductor structure[4]. We tune the system *in situ* through a quantum phase transition between two distinct states, each a version of the Kondo state[5], in which a bound electron interacts with surrounding mobile electrons. The boundary between these competing Kondo states is a quantum critical point—namely, the exotic and previously elusive two-channel Kondo state[6,7], in which electrons in two reservoirs are entangled through their interaction with a single localized spin.

The Kondo effect has become a hallmark of coherent electron transport in a variety of nanostructures, ranging from lithographically defined semiconductors to carbon nanotubes and molecules[8,9]. Kondo applied the phenomenological hamiltonian[10]

$$H_K = J\,\mathbf{s}\cdot\mathbf{S} + H_{\text{reservoir}} \qquad (1)$$

to describe a magnetic impurity embedded in a host sea of electrons. A localized spin $\mathbf{S}$ couples antiferromagnetically with strength J to spins $\mathbf{s}$ of electrons in the surrounding reservoir. $H_{\text{reservoir}}$ represents the free electrons in the reservoir. At temperatures below the Kondo temperature T_K, electrons in the reservoir screen the localized spin. The Kondo hamiltonian was later found to be derivable from the more microscopic Anderson model, which consists of an electron bound to an impurity site in a metal host (Fig. 1a). Here, Kondo's antiferromagnetic coupling emerges from tunnelling on and off the local site.

Many systems of strongly interacting particles can be understood in the framework of Landau's Fermi liquid theory, whose basic entities, termed quasiparticles, roll most effects of interactions into changes in particle properties, such as mass and energy. Although the Kondo ground state is complex, its excitations can still be described as weakly interacting quasiparticles. Some of the most intriguing problems in solid-state physics arise when this simplification cannot be applied. Examples of such highly correlated systems include Luttinger liquids, fractional quantum Hall Laughlin liquids, high-temperature superconductors, and the two-channel Kondo system, a novel state studied experimentally in this Letter.

In the two-channel Kondo (2CK) model, introduced 25 years ago in refs 6 and 7 independently, a localized spin $\mathbf{S}$ is antiferromagnetically coupled to two independent reservoirs of electrons according to the hamiltonian:

$$H_{2CK} = J_1\mathbf{s}_1\cdot\mathbf{S} + J_2\mathbf{s}_2\cdot\mathbf{S} + H_{\text{reservoirs}} \qquad (2)$$

The symmetric 2CK state is formed when the two independent channels (or reservoirs) are equally coupled to the magnetic impurity, that is, $J_1 = J_2$. Each reservoir individually attempts to screen the local spin. As they cannot both screen the spin, this is an unstable situation, resulting in a new ground state in which the local impurity is only partially screened. Unlike the situation for single-channel Kondo (1CK), in the 2CK state the quasiparticle concept of Fermi liquid theory does not apply: the decay rate for a low energy excitation ($\sim\sqrt{\varepsilon}$) is greater than the energy ε of the excitation itself. Stable low-lying excitations must thus be collective[2,11].

Any difference in channel coupling will force the system away from the non-Fermi-liquid 2CK state and towards the 1CK state associated with the more strongly coupled reservoir. Although the symmetric 2CK state might therefore seem difficult to access, it has been invoked to explain remarkable low-energy properties of some heavy fermion materials[12–14] and glassy metals[15–17]. However, the connections of these experimental observations to 2CK theory remain problematic, in part because the microscopic electronic structure of the various materials is unclear.

In this Letter, we present experimental results on an artificial impurity that is designed to display the 2CK effect. Crucially, we can precisely control the coupling constants J_1 and J_2, while maintaining the independence of the two channels. The system is built from a GaAs/AlGaAs heterostructure containing a low density ($n_e = 2\times10^{11}\,e^-\,cm^{-2}$), high mobility ($\mu = 2\times10^6\,cm^2\,V^{-1}\,s^{-1}$) two-dimensional electron gas (2DEG) 68 nm below the surface. We follow the proposal of ref. 4 to produce two independent screening channels for an artificial magnetic impurity. A gate-defined quantum dot containing ~25 electrons in an area of 0.04 μm^2 plays the role of our magnetic impurity (Fig. 1d, left). Its bare charging energy $U \approx 1$ meV and its average single-particle level spacing $\Delta \approx 100$ μeV. Previous experiments that claim to probe 2CK behaviour[12–17] used a local orbital degeneracy in place of spin, freeing spin of the surrounding conduction electrons to act as the channel index. In contrast, our local degeneracy is a real spin, and we use two physically separated reservoirs (red and blue in Fig. 1d) for the screening channels. Two leads of the small quantum dot cooperate as a single screening channel with antiferromagnetic coupling J_{ir} ('infinite reservoir')[18]. An additional lead is made finite in size (red, Fig. 1d), so that adding or removing an electron from this reservoir is energetically forbidden at low temperature, a phenomenon known as Coulomb blockade. The area of the finite reservoir is ~3 μm^2, corresponding to a charging energy $E_c = 100$ μeV ≈ 1.2 K, and a single-particle level spacing $\Delta_{fr} = 2$ μeV ≈ 25 mK ('finite reservoir'). This level spacing is only slightly larger than the base electron temperature of our dilution refrigerator (12 mK, as determined by Coulomb blockade thermometry on the small quantum dot), and indeed we cannot resolve these levels even at base temperature. Hence, the finite reservoir has an effectively continuous density of states and can screen the magnetic impurity. As Coulomb blockade prevents exchange of electrons with the other leads, the finite reservoir acts as a second Kondo screening channel (Fig. 1e), with antiferromagnetic coupling J_{fr},

[1]Department of Physics, [2]Department of Applied Physics, Stanford University, Stanford, California 94305, USA. [3]Department of Physics, Harvard University, Cambridge, Massachusetts 02138, USA. [4]Department of Condensed Matter Physics, Weizmann Institute of Science, Rehovot 96100, Israel. †Present address: Advanced Micro Devices, Austin, Texas 78741, USA.

allowing the possibility of observing and studying the 2CK effect. The 2CK hamiltonian (equation (2)) has three possible ground states, depending on the relative couplings to the two reservoirs: 1CK with the finite reservoir ($J_{fr} > J_{ir}$), 1CK with the infinite reservoir ($J_{ir} > J_{fr}$), and 2CK at the quantum critical point ($J_{fr} = J_{ir}$).

In Fig. 2, we demonstrate that the small quantum dot can act as a tunable magnetic impurity and display the 1CK effect. If the small quantum dot has an odd number of electrons, it has a net spin and acts as a magnetic impurity. With gate 'n' de-energized (0 V), the system has three conventional leads (blue and red in Fig. 1d), all of which cooperate to screen the magnetic impurity with a single energy scale kT_K. At temperature $T \lesssim T_K$, the Kondo effect enhances scattering and hence conductance from one lead to another. We measure the conductance $g \equiv dI/dV_{ds}|_{V_{ds}=0}$ between the two blue leads (I is current, and V_{ds} is voltage between source and drain reservoirs). As temperature is increased, the Kondo state is partially destroyed, so the conductance decreases (Fig. 2b). The conductance as a function of temperature (for example, Figure 2b inset) matches the expected form $g(T)$ for a quantum dot in the Kondo regime[19,20]; see Supplementary Information for complete analysis. This, and all other measurements reported here, are performed in a magnetic field $B = 130$ mT normal to the plane of the heterostructure. The orbital effect of this modest field suppresses direct transmission through the small quantum dot, which we found to yield Fano lineshapes at zero magnetic field (compare ref. 21). Owing to the small g-factor of electrons in GaAs/AlGaAs heterostructures, $|g| \approx 0.4$, the Zeeman effect of the field is unimportant in both 1CK and 2CK regimes (see Supplementary Information for details). All results presented in this Letter are for this same electron occupancy, although we have observed similar behaviour in the next Kondo valley (two fewer electrons in the small dot), as well as on thermally cycling the device.

Figure 3 explores the effect of energizing gate 'n', thus forming the finite reservoir. Differential conductance $g(T, V_{ds}) = dI/dV_{ds}$ is enhanced near zero bias (Fig. 3b and f) when the electrostatic potential of the small dot is set to the middle of the Kondo valleys in Fig. 2b or c, respectively. This is a manifestation of the enhanced density of states at the Fermi level, widely accepted as one of the classic signatures of the Kondo effect, demonstrating clearly that the small dot acts as a magnetic impurity. Remarkably, the zero-bias enhancement changes to zero-bias suppression as gate n is made more negative, closing off the big dot to form a finite reservoir with integer occupancy (Fig. 3g). The change signals that the single-channel Kondo state with the leads has been broken, to form instead solely with the finite reservoir. This occurs for $J_{fr} > J_{ir}$, as shown in more detail in Fig. 3h and Supplementary Information. With slightly weaker coupling to the finite reservoir (Fig. 3c), $J_{ir} > J_{fr}$, the Kondo state is formed solely with the infinite reservoir. This effect requires the finite reservoir to have integer occupancy, that is, the device must be set to a Coulomb blockade valley of the finite reservoir.

In Fig. 3d and h, we provide further evidence that, with the finite reservoir formed, two independent 1CK states can exist, depending on the relative coupling of the small dot to the two reservoirs. We

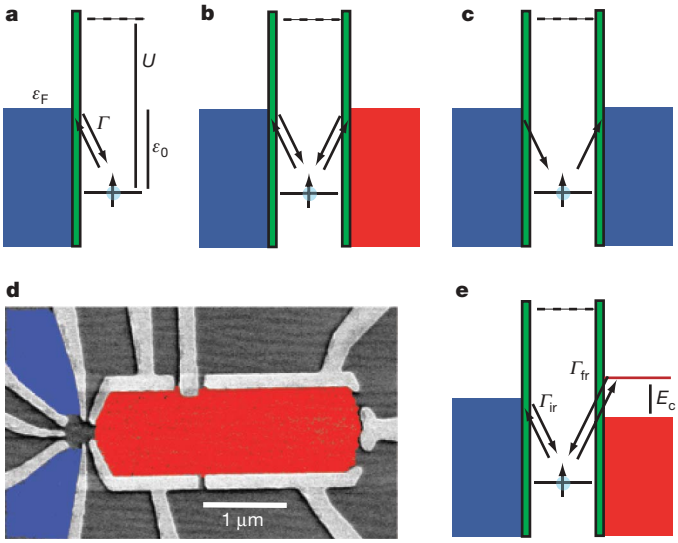

Figure 1 | One and two-channel Kondo effects. a, Single channel Kondo (1CK) effect. The Anderson model describes a magnetic impurity in a metal as a single spin-degenerate state (right side of green barrier) coupled to a Fermi reservoir of electrons (left) with Fermi energy ε_F. Coulomb interaction U between localized electrons favours having only a single electron in the localized state. The antiferromagnetic coupling J between the localized spin and the reservoir depends on the tunnelling rate Γ, the depth of the level ε_0, and U, according to $J \propto \Gamma U/[\varepsilon_0(\varepsilon_0 + U)]$ (ref. 30). At low temperature, high-order tunnelling processes between the local state and the Fermi reservoirs coherently add together to screen the localized electron spin. **b**, Two channel Kondo (2CK) effect. A localized electron is now coupled to two independent Fermi reservoirs (blue and red). If the two independent reservoirs are equally coupled to the localized spin, each will individually attempt to screen the spin, resulting in the formation of a highly correlated electron state. **c**, Physically separating two reservoirs does not suffice to make them independent. If a localized electron can hop off the site to the right reservoir and a new electron can hop onto the site from the left, the two reservoirs will cooperate in screening the localized spin. To create two independent screening channels, processes that transfer electrons from one reservoir to another must be suppressed. **d**, Experimental realization of the 2CK effect. We add an additional finite reservoir (red) to an artificial magnetic impurity connected to an infinite reservoir composed of two conventional leads (blue). **e**, Coulomb blockade suppresses exchange of electrons between the finite reservoir and the normal leads at low temperature. The two reservoirs (blue and red) hence act as two independent screening channels (see main text).

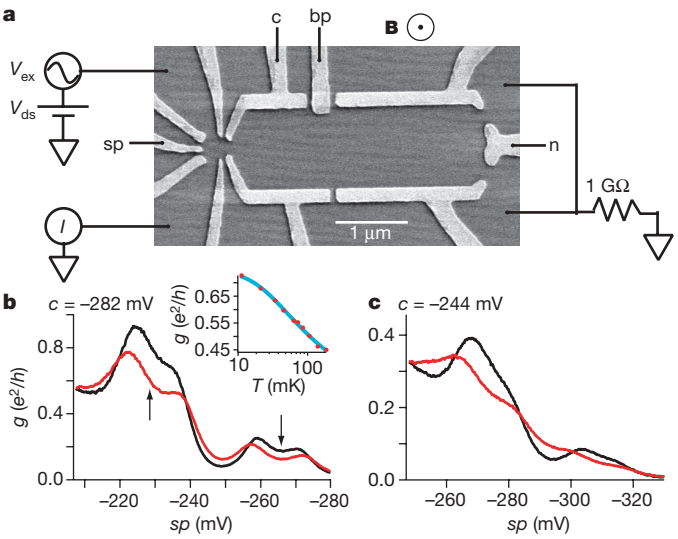

Figure 2 | Artificial magnetic impurity. a, Scanning electron micrograph of a device similar to that measured. The device consists of a small quantum dot (magnetic impurity, left) coupled to conventional leads (top and bottom left) and to a large quantum dot (finite reservoir, right). Electrons are depleted under every gate by application of negative voltages. In the experiments described here, voltages are varied on gates labelled c ('coupling' between dots), bp ('big dot plunger'), sp ('small dot plunger') and n ('nose', which opens or closes the big dot). All transport measurements presented in Figs 3 and 4 are measured with source and drain connected as shown, in a magnetic field of 130 mT normal to the plane of the 2DEG. **b**, With gate voltage $n = 0$, the large dot opens into an infinite reservoir. Arrows mark regions where the small dot has an unpaired spin, leading to enhanced conductance at 12 mK (black) compared to 50 mK (red). Fitting the temperature dependence of the conductance (**b** inset), we find that the Kondo temperature ranges from 110 to 300 mK (see Supplementary Information). In **c**, the data from **b** are shown for stronger tunnel coupling to the right lead: $c = -244$ mV instead of -282 mV. From the temperature dependence of **c**, we find that T_K ranges from 180 to 320 mK.

have fine control of the occupancy of both the finite reservoir and the small dot with gates bp and sp (see Fig. 2 for gates; this fine control is demonstrated in Supplementary Information). The differential conductance $g(V_{ds}, T)$ of a 1CK system is expected to follow a specific form as a function of both bias and temperature, at an energy scale substantially below kT_K (ref. 22):

$$\frac{g(0,\ T)-g(V_{ds},\ T)}{T^{\alpha}}=\kappa\left(\frac{eV_{ds}}{kT}\right)^{2} \qquad (3)$$

where the exponent $\alpha = 2$ is characteristic of 1CK behaviour, and $\kappa = 0.82g_0/T_K^2$. The numerical prefactor of order unity is dependent on the underlying model, numerical calculations, and proximity to the symmetric 2CK fixed point (see Supplementary Information), so we simply treat κ as a free fitting parameter for each set of gate voltages. Figure 3d demonstrates excellent 1CK scaling at temperatures of 12, 24, 28 and 38 mK, all well below T_K. A nonlinear fit to the data in Fig. 3d yields $\alpha = 1.72 \pm 0.40$ (95% confidence limits), consistent with $\alpha = 2$.

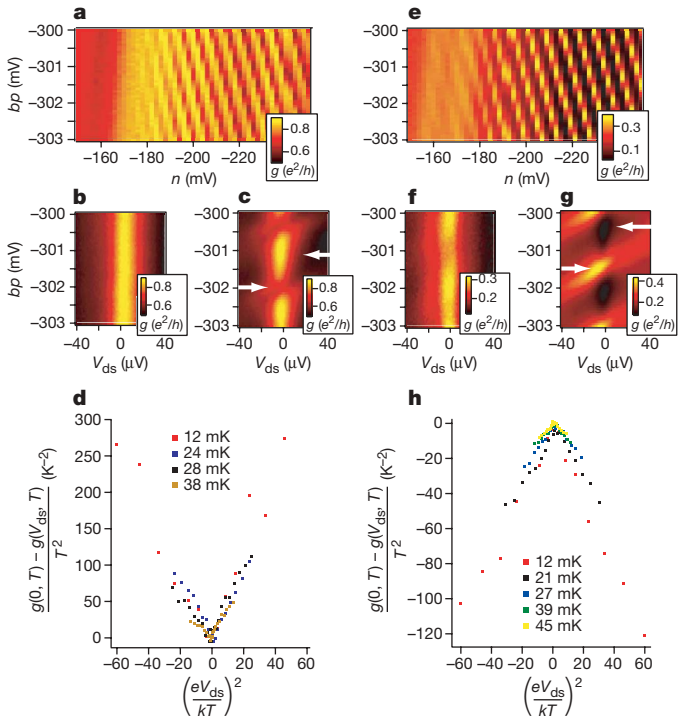

Figure 3 | The formation of two competing 1CK states with two different reservoirs. **a**, *sp* is set so that the small dot has an unpaired spin (middle of a Kondo valley), and *c* is set to −282 mV. Conductance is shown as a function of *n* and *bp*. With $n > -180$ mV, varying *bp* has little effect on the conductance. As *n* is made more negative, the reservoir becomes finite and a series of stripes in the conductance map reflects Coulomb blockade in the finite reservoir (see Supplementary Information for explanation of the modulation). In **b** and **c**, differential conductance as a function of bias (V_{ds}) and *bp* is shown for $n = -170$ mV and $n = -224$ mV, respectively. In **b**, there is clear zero-bias enhancement, consistent with the Kondo effect. In **c**, the zero-bias enhancement (denoted by the right-hand arrow) is modulated by the charge state of the finite reservoir (see Supplementary Information). The left-hand arrow marks the charge degeneracy point of the finite reservoir. **d**, Plotting a specific combination of temperature and bias collapses the data for a single point in occupancy of the two dots (small dot with odd occupancy and large dot in Coulomb blockade; $T_K = 175$ mK, $g_0 = 0.75e^2/h$) onto a single V-shaped curve, corresponding to the scaling relation predicted for 1CK behaviour (equation (3)). **e**, Same as **a**, except with stronger interdot coupling: $c = -244$ mV. **f**, As in **b**, we observe a clear zero-bias conductance enhancement for $n = -170$ mV. **g**, However, in this case at $n = -224$ mV the zero-bias enhancement is replaced by zero-bias suppression (denoted by the right-hand arrow). Here the local spin forms a Kondo state with the finite reservoir, suppressing conductance through the small quantum dot (see main text). Again, the zero-bias feature is modulated by the charge state of the finite reservoir, and the left-hand arrow marks a charge degeneracy point of the finite reservoir. **h**, We collapse differential conductance data at a single point in (*sp*, *bp*) onto a single inverted V-shaped curve using the same temperature–bias scaling as in **d**. Deviations from perfect scaling may be related to the slightly lower Kondo temperature ($T_K = 120$ mK, $g_0 = 0.16e^2/h$.)

In Fig. 3h, we demonstrate that at stronger coupling to the finite reservoir ($J_{fr} > J_{ir}$), the small dot forms a Kondo state with the finite reservoir, as manifested by low-energy suppression rather than enhancement of conductance between the normal leads of the small dot (see Supplementary Information for analysis of temperature dependence). Using the same scaling relation as above (equation (3)), the data again collapse onto a single (inverted) curve at low bias and temperature (Fig. 3h). Interestingly, we find the numerical prefactor of κ to be 0.25 in both 1CK regimes—precisely matching each other, but only roughly agreeing with our predicted value of 0.82.

Having established the existence of two distinct Kondo ground states—depending on the ratio J_{ir}/J_{fr}—we next demonstrate the tunability necessary to reach the symmetric 2CK state, $J_{ir} \approx J_{fr}$. By setting the tunnel coupling to the finite reservoir to an intermediate value, we can observe either zero-bias enhancement or zero-bias suppression (marked by white arrows in Fig. 4a), in both cases away from any charge degeneracy point of the finite reservoir (marked by a black arrow in Fig. 4a). This is expected[4], as the antiferromagnetic coupling to a reservoir depends not only on a tunnelling rate but also on the energy required to transfer an electron from the local site to that reservoir. Gate bp tunes that addition energy for the finite reservoir, modifying J_{fr} while keeping J_{ir} nearly constant. The region in (*sp*, *bp*)—we use *sp* to indicate the voltage on gate sp, and so on)—of suppressed conductance (red) grows rapidly with increasing coupling to the finite reservoir, as seen in Fig. 4b, c and d for $c = -258$, -256 and -254 mV, respectively.

The evolution of dI/dV_{ds} from zero-bias enhancement to zero-bias suppression as a function of the voltage on coupling gate c may be seen most clearly in Fig. 4e. We identify the curve for $c = -260$ mV as being very close to the 2CK symmetric point. At first sight, it is surprising that this curve does not display a clear cusp at low V_{ds} ($G \propto 1 - \text{const.}\sqrt{V_{ds}}$). In fact, conformal field theory predicts that at the 2CK symmetric point the differential conductance should depend quadratically on bias for $eV_{ds} < kT$, and should only cross over to $\sqrt{V_{ds}}$ behaviour at higher bias $eV_{ds} > 3kT$ (see green curve in Fig. 4f). Such a crossover is hard to see in a single plot of differential conductance versus bias. Instead, we combine the dependence of differential conductance on both bias and temperature in a scaling plot to produce compelling evidence for 2CK behaviour. The expected scaling form is somewhat different from that for 1CK[11,16,23]:

$$\frac{g(0,\ T)-g(V_{ds},\ T)}{T^{\alpha_2}}=\kappa_2\,Y\left(\frac{eV_{ds}}{kT}\right) \qquad (4)$$

Here $\alpha_2 = 0.5$, $\kappa_2 = (g_0/2)(\pi/T_{2CK})^{\alpha_2}$, and

$$Y(x)=1-F_{2CK}(x/\pi)\approx\begin{cases}\frac{3}{\pi}\sqrt{x}-1 & \text{for}\quad x\gg 1\\ cx^2 & \text{for}\quad x\ll 1\end{cases} \qquad (5)$$

with $c \approx 0.0758$ (ref. 24). As with κ in the 1CK analysis, in practice we treat κ_2 as a free parameter for each set of gate voltages. F_{2CK}, the dependence of 2CK conductance on normalized bias, is found by conformal field theory[11,25,26].

Figure 4f shows that when we tune close to the 2CK symmetric point ($c = -258$ mV rather than -260 mV, due to a small shift in parameters), data at various temperatures and biases collapse onto each other and match the conformal field theory prediction (equation (4)), which is scaled vertically by κ_2. The horizontal axis is plotted as $(eV_{ds}/kT)^{0.5}$, to emphasize that $g(V_{ds}) \propto 1 - \text{const.}\sqrt{V_{ds}}$ for $eV_{ds}/kT \gg 1$.

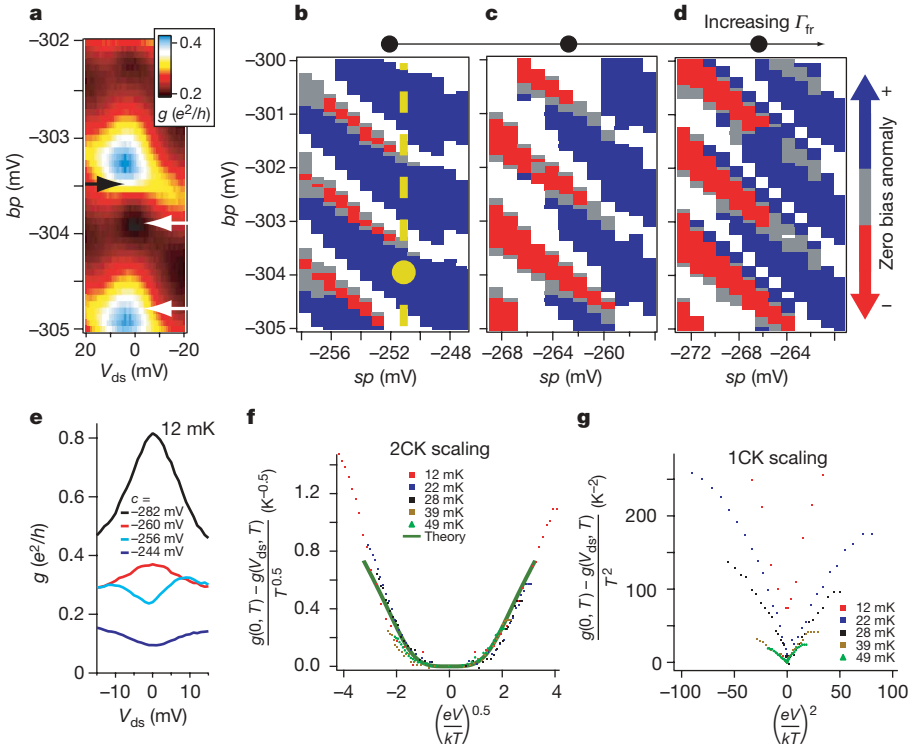

Figure 4 | Evidence for 2CK physics. **a**, Differential conductance as a function of *bp* and V_{ds} in the middle of a Kondo valley, with intermediate coupling to the finite reservoir, $c = -258$ mV. In contrast to Fig. 3c and g, here we observe both zero-bias enhanced and zero-bias suppressed conductance (marked by bottom and top white arrows, respectively) by fine-tuning *bp*. The black arrow marks the charge degeneracy point of the finite reservoir. **b–d**, At $c = -258$, -256 and -254 mV, conductance may be either enhanced or suppressed at zero bias, depending on the fine tuning of the electrostatic potentials of the small dot and finite reservoir with gates *sp* and *bp*, respectively. Red and blue indicate regions of suppressed conductance or enhanced conductance, respectively, while grey indicates relatively flat conductance around $V_{ds} = 0$. White regions are too close to charge degeneracy of dot or finite reservoir to diagnose Kondo-induced enhancement or suppression of conductance. Increased coupling to the finite reservoir expands the region of suppressed conductance (red). The yellow dashed line in **b** shows the setting of *sp* used in **a**, and the yellow dot shows the approximate location in the charging hexagon of the symmetric 2CK point analysed in **f** and **g**. **e**, Differential conductance near zero bias evolves with coupling *c* from zero-bias enhancement to zero-bias suppression. For each curve, *sp* sets the small dot in the middle of a Kondo valley and *bp* sets the finite reservoir midway between two charge degeneracy points. **f**, **g**, Tuning *bp* near -304.7 mV (bottom white arrow in **a**), we observe that differential conductance depends on bias and temperature with $\alpha = 0.5$, consistent with 2CK (**f**) and inconsistent with 1CK (**g**, which attempts to apply scaling to exactly the same data, but with $\alpha = 2$.) In the Supplementary Information we show the converse, namely that in the 1CK region the 2CK scaling law does not fit, while the 1CK scaling does. A two-dimensional nonlinear fit to the data set used for **f** and **g** yields $\alpha_2 = 0.62 \pm 0.21$, consistent with $\alpha = 0.5$.

In Fig. 4g we show the same data scaled as would be appropriate for 1CK behaviour (equation (3)) instead of 2CK. As anticipated, this scaling fails completely: scaled data for different temperatures deviate from each other even near zero bias. A two-dimensional nonlinear fit to the data in Fig. 4f produces a value $\alpha_2 = 0.62 \pm 0.21$ (95% confidence limits), consistent with 2CK behaviour. Naively, we would expect 2CK behaviour to persist only up to $\{kT, eV_{ds}\} \approx (kT_K)^2/E_c \approx 1.7\,\mu$eV (ref. 27). Empirically, 2CK persists to much higher energies: conductance follows the 2CK scaling form up to $V_{ds} = 15\,\mu$eV, corresponding to $T = 180$ mK, even higher than T_K. Enhancement of 2CK energy scales has been predicted in our geometry in the presence of charge fluctuations[28], but is not expected to be so dramatic for our parameter values.

Here we have presented data demonstrating the existence of two independent 1CK states, along with a study of the associated 2CK state. Remarkably, the conductance of the symmetric 2CK state matches not only a simple power law but rather a complete theoretically calculated non-Fermi-liquid scaling function over a broad range of energy (equation (5), Fig. 4f). In future, it would be interesting to extend this scaling form theoretically and experimentally to cover the effects of a Zeeman field and slightly asymmetric coupling to the two reservoirs—for example, to quantitatively describe the family of curves in Fig. 4e. Finally, other parameter regimes of the same structure may show additional exotic behaviour[28,29].

Received 7 June; accepted 28 December 2006.

1. Pruschke, T., Jarrel, M. & Freericks, J. Anomalous normal-state properties of high T_c superconductors: Intrinsic properties of strongly correlated electron systems? *Adv. Phys.* **44**, 187–210 (1995).
2. Cox, D. L. & Zawadowski, A. Exotic Kondo effects in metals: magnetic ions in a crystalline electric field and tunnelling centres. *Adv. Phys.* **47**, 599–942 (1998).
3. Hanson, R., Kouwenhoven, L. P., Petta, J. R., Tarucha, S. & Vandersypen, L. M. K. Spins in few-electron quantum dots. Preprint at ⟨http://arxiv.org/cond-mat/0610433⟩ (2006).
4. Oreg, Y. & Goldhaber-Gordon, D. Two-channel Kondo effect in a modified single electron transistor. *Phys. Rev. Lett.* **90**, 136602 (2003).
5. Wilson, K. G. The renormalization group: critical phenomena and the Kondo problem. *Rev. Mod. Phys.* **47**, 773–840 (1974).
6. Nozières, P. & Blandin, A. Kondo effect in real metals. *J. Phys.* **41**, 193–211 (1980).
7. Zawadowski, A. Kondo-like state in a simple model for metallic glasses. *Phys. Rev. Lett.* **45**, 211–214 (1980).
8. Goldhaber-Gordon, D. *et al.* Kondo effect in a single-electron transistor. *Nature* **391**, 156–159 (1998).
9. Grobis, M., Rau, I. G., Potok, R. M. & Goldhaber-Gordon, D. Kondo effect in mesoscopic quantum dots. Preprint at ⟨http://arxiv.org/cond-mat/0611480⟩ (2006).
10. Kondo, J. Resistance minimum in dilute magnetic alloys. *Prog, Theor. Phys.* **32**, 37–49 (1964).
11. Affleck, I. & Ludwig, A. W. W. Exact conformal-field-theory results on the multichannel Kondo effect: single-fermion Green's function, self-energy, and resistivity. *Phys. Rev. B* **48**, 7297–7321 (1993).
12. Cox, D. L. Quadrupolar Kondo effect in uranium heavy-electron materials. *Phys. Rev. Lett.* **59**, 1240–1243 (1987).

13. Seaman, C. L. *et al.* Evidence for non-Fermi-liquid behavior in the Kondo alloy $Y_{1-x}U_xPd_3$. *Phys. Rev. Lett.* **67,** 2882–2885 (1991).
14. Besnus, M. J. *et al.* Specific-heat and NMR of the Kondo system $YbPd_2Si_2$. *J. Magn. Magn. Mater.* **76–7,** 471–472 (1988).
15. Ralph, D. C. & Buhrman, R. A. Observations of Kondo scattering without magnetic-impurities — a point contact study of 2-level tunneling systems in metals. *Phys. Rev. Lett.* **69,** 2118–2121 (1992).
16. Ralph, D. C., Ludwig, A. W. W., von Delft, J. & Buhrman, R. A. 2-channel Kondo scaling in conductance signals from 2-level tunneling systems. *Phys. Rev. Lett.* **72,** 1064–1067 (1994).
17. Cichorek, T. *et al.* Two-channel Kondo effect in glasslike ThAsSe. *Phys. Rev. Lett.* **94,** 236603 (2005).
18. Glazman, L. I. & Raikh, M. E. Resonant Kondo transparency of a barrier with quasilocal impurity states. *JETP Lett.* **47,** 452–455 (1988).
19. Costi, T. A. & Hewson, A. C. Transport coefficients of the Anderson model via the numerical renormalization group. *J. Phys. Condens. Matter* **6,** 2519–2558 (1994).
20. Goldhaber-Gordon, D. *et al.* From the Kondo regime to the mixed-valence regime in a single-electron transistor. *Phys. Rev. Lett.* **81,** 5225–5228 (1998).
21. Göres, J. *et al.* Fano resonances in electronic transport through a single-electron transistor. *Phys. Rev. B* **62,** 2188–2194 (2000).
22. Majumdar, K., Schiller, A. & Hershfield, S. Nonequilibrium Kondo impurity: Perturbation about an exactly solvable point. *Phys. Rev. B* **57,** 2991–2999 (1998).
23. Hettler, M. H., Kroha, J. & Hershfield, S. Nonlinear conductance for the two channel Anderson model. *Phys. Rev. Lett.* **73,** 1967–1970 (1994).
24. Oreg, Y. & Goldhaber-Gordon, D. *Physics of Zero and One Dimensional Nanoscopic Systems* (Springer Series in Solid State Sciences, Springer, in the press).
25. Pustilnik, M., Borda, L., Glazman, L. & von Delft, J. Quantum phase transition in a two-channel-Kondo quantum dot device. *Phys. Rev. B* **69,** 115316 (2004).
26. von Delft, J., Ludwig, A. W. W. & Ambegaokar, V. The 2-channel Kondo model. II. CFT calculation of non-equilibrium conductance through a nanoconstriction containing 2-channel Kondo impurities. *Ann. Phys.* **273,** 175–241 (1999).
27. Florens, S. & Rosch, A. Climbing the entropy barrier: Driving the single- towards the multichannel Kondo effect by a weak Coulomb blockade of the leads. *Phys. Rev. Lett.* **92,** 216601 (2004).
28. Lebanon, E., Schiller, A. & Anders, F. B. Enhancement of the two-channel Kondo effect in single-electron boxes. *Phys. Rev. B* **68,** 155301 (2003).
29. Le Hur, K., Simon, P. & Borda, L. Maximized orbital and spin Kondo effects in a single-electron transistor. *Phys. Rev. B* **69,** 045326 (2004).
30. Haldane, F. D. M. Scaling theory of the asymmetric Anderson model. *Phys. Rev. Lett.* **40,** 416–419 (1978).

Supplementary Information is linked to the online version of the paper at www.nature.com/nature.

Acknowledgements We thank A. Schiller, E. Lebanon, F. Anders, I. Affleck, T. Costi, L. Glazman, K. Le Hur, C. Marcus, M. Pustilnik, E. Sela, J. von Delft and G. Zarand for discussions. E. Lebanon and F. Anders also performed NRG calculations that gave us crucial intuition regarding where our experimental system was in parameter space. S. Roy helped us understand how to perform nonlinear fits to determine the exponents α and α_2 for the energy dependence in both 1CK and 2CK regimes. This work was supported by an NSF CAREER Award, a US-Israel BSF Award, DIP and ISF. D.G.-G. acknowledges Fellowships from the Sloan and Packard Foundations, and a Research Corporation Research Innovation Award. R.M.P. was supported by an ARO Graduate Fellowship during the early stages of this work.

Author Information Reprints and permissions information is available at www.nature.com/reprints. The authors declare no competing financial interests. Correspondence and requests for materials should be addressed to D.G-G. (goldhaber-gordon@stanford.edu).